Brain Struct Funct
DOI 10.1007/s00429-013-0664-x

ORIGINAL ARTICLE

MeCP2-mediated alterations of striatal features accompany psychomotor deficits in a mouse model of Rett syndrome

Fang-Chi Kao · San-Hua Su · Gregory C. Carlson · Wenlin Liao

Received: 16 August 2013 / Accepted: 15 October 2013

Abstract Rett Syndrome (RTT) is a neurodevelopmental disorder caused by mutations in the methyl-CpG-binding protein 2 (*MECP2*) gene. Affected individuals develop motor deficits including stereotypic hand movements, impaired motor learning and difficulties with movement. To understand the neural mechanisms of motor deficits in RTT, we characterized the molecular and cellular phenotypes in the striatum, the major input nucleus of the basal ganglia that controls psychomotor function, in mice carrying a null allele of *Mecp2*. These mice showed significant hypoactivity associated with impaired motor coordination and motor skill learning. We found that dopamine content was significantly reduced in the striatum of *Mecp2* null mice. Reduced dopamine was accompanied by down-regulation of tyrosine hydroxylase and up-regulation of dopamine D2 receptors, particularly in the rostral striatum. We also observed that loss of MeCP2 induced compartment-specific alterations in the striatum, including reduced expression of μ-opioid receptors in the striosomes and increased number of calbindin-positive neurons in the striatal matrix. The total number of parvalbumin-positive interneurons and their dendritic arborization were also significantly increased in the striatum of *Mecp2* null mice. Together, our findings support that MeCP2 regulates a unique set of genes critical for modulating motor output of the striatum, and that aberrant structure and function of the striatum due to MeCP2 deficiency may underlie the motor deficits in RTT.

Keywords Autism spectrum disorders · Striatum · Dopamine · μ-Opioid receptor · Calbindin · Parvalbumin

F.-C. Kao and S.-H. Su contributed equally to this work.

F.-C. Kao · S.-H. Su · W. Liao (✉)
Institute of Neuroscience, National Cheng-Chi University, 64, Sec. 2, Chi-Nan Road, Wen-Shan District, Taipei 11605, Taiwan
e-mail: wlliao@nccu.edu.tw

G. C. Carlson
Department of Psychiatry, University of Pennsylvania, Philadelphia, PA 19104, USA

W. Liao
Research Center for Mind, Brain and Learning, National Cheng-Chi University, Taipei 11605, Taiwan

Introduction

Movement control is the basis of behaviors. Studies on the pathogenesis of movement disorders provide insights into neural control of behaviors and aid in the development of therapeutic interventions. In children with autism spectrum disorders (ASDs), enhanced stereotypy and dyspraxia are closely associated with inappropriate control of voluntary movement (Sterling et al. 2011; Mosconi et al. 2011). Rett Syndrome (RTT, OMIM #312750) is an ASD that primarily affects females with an estimated prevalence of one in ~10,000 births. Girls with RTT develop normally for the first 6–18 months after birth, followed by behavioral regression such as loss of learned motor and language skills, onset of autistic behaviors, breathing abnormalities, and occasional seizures (Hagberg et al. 1983). Most RTT patients also show stereotypic hand movements, impaired motor learning and difficulties with movement. These motor symptoms usually exacerbate with age and resemble Parkinson's disease later in life (Chahrour and Zoghbi 2007; Temudo et al. 2008).

Mutations of the X-linked gene encoding methyl-CpG-binding protein 2 (MeCP2), which is a transcriptional

Published online: 12 November 2013

regulator (Nan et al. 1998; Chahrour et al. 2008), have been identified as the major cause of RTT (Amir et al. 1999). The MeCP2 protein is ubiquitously expressed throughout the body, but is highly enriched in mature neurons (Shahbazian et al. 2002a). *Mecp2* null mice and mice carrying truncated or deficient MeCP2 protein recapitulate many RTT-like symptoms including late onset of hypoactivity, irregular breathing, and deficits in motor coordination (Guy et al. 2001; Chen et al. 2001; Shahbazian et al. 2002b; Goffin et al. 2012). Notably, forebrain-specific deletion of *Mecp2* leads to similar deficits in motor coordination as those observed in *Mecp2* null mice (Gemelli et al. 2006), suggesting that the pathological origin for motor symptoms of RTT may be located in the forebrain. In the frontal motor cortex, loss of MeCP2 has been shown to reduce synaptic strength of excitatory intracortical connections in both *Mecp2* knockdown model and *Mecp2* null mice (Wood et al. 2009; Wood and Shepherd 2010), however, the subcortical areas in the forebrain controlling voluntary movement have yet been characterized in *Mecp2* null mice.

The striatum is the major input nucleus of the basal ganglia and the most prominent subcortical area known to control voluntary movement in the forebrain. Medium spiny neurons (MSNs) are the projection neurons that constitute about 98 % of neurons in the striatum. They integrate glutamatergic excitatory inputs from the frontal motor cortex and dopaminergic afferents from the substantia nigra pars compacta (SNpc). MSNs also project inhibitory GABAergic efferents back to the substantia nigra pars reticularta (SNpr) and motor thalamic areas through the "direct" or "indirect" pathway to modulate execution of cortical motor command (Kreitzer and Malenka 2008). Anatomically, the striatal MSNs are organized by two distinct compartments, the striosomes (also called patches) and the surrounding matrix, where neurons are born at different embryonic stages, express alternative marker genes, and connect to different cortical and midbrain areas (Fujiyama et al. 2006; Watabe-Uchida et al. 2012). In comparison to the matrix neurons, the striosomal neurons are highly enriched within the rostral striatum and receive compartment-specific innervations from the dopaminergic midbrain area during development, suggesting that structural and functional differences exist along the rostral–caudal axis of the striatum (Graybiel 1984; Liao et al. 2008). Physiologically, MSN activity is modulated by numerous classes of striatal interneurons. The fast-spiking parvalbumin (PV)-expressing interneurons make inhibitory synapses onto the MSNs and evoke large inhibitory postsynaptic potentials, and hence effectively delay or suppress the firing of MSNs and lead to feed-forward modulation of striatal output (Koos and Tepper 1999). Notably, a number of neurodevelopmental and psychiatric disorders with psychomotor deficits, such as autism, schizophrenia, attention deficits hyperactivity disorders, obsessive compulsive disorders, and drug addiction, have all been linked to malfunction of the striatum (Kreitzer and Malenka 2008; Crittenden and Graybiel 2011). However, the roles of the striatum in the etiology of motor deficits in RTT remain to be determined.

Given the functional relevance of the striatum to motor control, we hypothesized that the motor dysfunction caused by MeCP2 deficiency is associated with aberrant striatal features. In the present study, we thus characterized the molecular and cellular phenotypes of the striatum in *Mecp2* null mice. We found that motor deficits in *Mecp2* null mice are accompanied by decreased dopamine levels, increased number of PV-positive interneurons, and altered expression of multiple genes involved in dopamine signaling and compartmentalization of the striatum. Importantly, we observed that the effects of *Mecp2* deletion differ along the rostral–caudal axis of the striatum with multiple molecular markers more strikingly affected in the rostral striatum compared with the caudal striatum. Our data suggest that alterations in the structure and function of the striatum caused by loss of MeCP2 may underlie the psychomotor deficits in RTT.

Methods

Animals

Male hemizygous *Mecp2* null mice ($Mecp2^{-/y}$, KO), female heterozygotes ($Mecp2^{+/-}$), and their wild-type (WT) littermate controls ($Mecp2^{+/y}$, $Mecp2^{+/+}$) were generated by crossing heterozygous $Mecp2^{+/-}$ females ($Mecp2^{tm1.1\ Bird}$, the Jackson Laboratory, USA) (Guy et al. 2001) with WT male mice (*C57BL/6J*, National Laboratory Animal Center, Taiwan). For behavioral testing, 4- to 5-week-old male and female mice and 10- to 12-week-old female mice were used. For neurochemical examination, only 4- to 5-week-old male mice were analyzed. All mice used in this study were maintained in a *C57BL/6J* background and housed in individual ventilation cages (Alternative Design, USA) at 22 ± 2 °C and 60 ± 10 % humidity under a 12-h light/dark cycle (light on 08:00–20:00). Food and water were available ad libitum. All experiments were approved by the Institutional Animal Care and Use Committee at National Cheng-Chi University.

Genotyping

Mice were weaned and ear-tagged at postnatal days 21–23, and genotyped by polymerase chain reaction (PCR) with the REDExtract-N-AmpTM Tissue PCR Kit (Sigma) as described (Miralves et al. 2007). Briefly, mouse tail tissues

Table 1 Primer sequences used in this study

Gene	Primer	Sequence
Mecp2	WT-FW	5′-GACCCCTTGGGACTGAAGTT-3′
	KO-FW	5′-CCATGCGATAAGCTTGATGA-3′
	RV	5′-CCACCCTCCAGTTTGGTTTA-3′
Th	Forward	5′-CCGGTGTACTTCGTGTCAGAG-3′
	Reverse	5′-AGGGTGTACGGGTCAAACTTC-3′
Drd1	Forward	5′-CTAATGAGCTGTGCCTCATCG-3′
	Reverse	5′-AGTGATGCTGATGGCTTTGTG-3′
Drd2	Forward	5′-AGATGCTTGCCATTGTTCTTG-3′
	Reverse	5′-TAGAGGACTGGTGGGATGTTG-3′
Mor1	Forward	5′-ATCCTTCTCCGACTCATGTTG-3′
	Reverse	5′-ACCAGCTCATCCCTGTGTTC-3′
CB	Forward	5′-GCCAGGTTACTACCAGTGCAG-3′
	Reverse	5′-TCTATGTATCCGTTGCCATCC-3′
Hprt	Forward	5′-CAAACTTTGCTTTC CCTGGTT-3′
	Reverse	5′-CAAAGTCTGGCCTGTATCCAA-3′
Irak1	Forward	5′-GTCTTGGATAGCCTGCAACTG-3′
	Reverse	5′-TGAGGGATTTGTCAGAGTGAA-3′

were incubated in 100 µl mixtures of extraction solution and tissue preparation solution (4:1) at 55 °C for 20 min. Lysates were denatured at 95 °C for 3 min, followed by 4 °C for 5 min. Neutralization solution (80 µl) was added and mixed well. One microliter of lysate was used for PCR reaction. The primers for genotyping of *Mecp2*-null mice were WT-FW, KO-FW, and RV (Table 1). PCR amplification was performed at 94 °C for 5 min, followed by 35 cycles at 94 °C for 30 s, 64 °C for 40 s, and 72 °C for 40 s. PCR products of 411 and 458 bp were corresponded to WT and mutant alleles, respectively.

Behavioral assays

All the behavioral assays were performed in a sound-reduced room at the same time of a day (1:00–6:00 pm) by unbiased operators who were blinded to mouse genotypes.

Open-field activity

Mecp2 null mice and their WT littermate controls at 4–5 weeks of age were tested and videotaped within a clear Plexiglas open-field arena (40 × 40 × 25 cm) for 16 min under dim light. Parameters of locomotor activity, including total distance traveled, percentage of resting time, average and maximal locomotion velocity, and percentage of time spent in the center arena were analyzed for the last 12 min (from 3.5 to 15.5 min, excluding the first 3.5 min of habituation period) with the Smart® tracking system (Harvard, USA). Body movements at speeds under the detection threshold for locomotion (2 cm/s) were counted as resting. The performance of mutant mice was normalized by the average performance of WT mice (shown as % of WT). Differences between genotypes were analyzed by Student *t* test.

Accelerating rotarod task

Male and female mice at 4–5 weeks and females at 10–12 weeks of age were briefly trained at a constant speed of 4 rpm on the rotarod apparatus (LE8200, PanLab, Spain) for 30 s before the first test. Thirty minutes later, testing was performed at an accelerating speed (4–40 rpm within 5 min). Three testing trials were performed on each day for five consecutive days, with an intertrial interval of 30 min. The latency of a mouse falling off the rotating rod was recorded automatically by the stop-plate. The median of three trials on each test day was adopted for statistical analysis by two-way analysis of variance (ANOVA) followed by Bonferroni's test. To quantify the daily progress of motor learning performance, the motor learning index (MLI) was defined as the percentage of normalized progress (learned skills) in two consecutive days: MLI_n $(\%) = (T_n - T_{n-1})/T_{n-1} \times 100\ \%$, where T_n is the falling latency on the n^{th} testing day.

Preparation of the brain tissue

After behavioral testing, a group of the mice ($n = 4$–8 for each genotype) were sacrificed by cervical dislocation. Tissues from the rostral, middle, and caudal levels of the striatum (ST-r, ST-m, ST-c) and the cerebral cortex at the corresponding positions (CTX-r, CTX-m, CTX-c) were microdissected on ice upon the aid of stainless steel brain matrix (Ted Pella, USA) and punches (diameter: 1.5 mm for ST-r, CTX-r, CTX-m, and CTX-c; 1.75 mm for ST-m; 2.0 mm for ST-c; Ted Pella, USA) at Bregma coordinates +1.54, +0.86, and +0.14 mm, respectively. The nucleus accumbens (NAc, Bregma +1.54 mm) and ventral midbrain (VMB, Bregma −3.28 mm) were collected manually from the same animals according to the atlas (Paxinos and Franklin 2004; Fig. 2a). Tissues were quickly frozen in liquid nitrogen and then kept at −80 °C until further analysis by high-performance liquid chromatography (HPLC), quantitative reverse transcription polymerase chain reaction (qRT-PCR) or western blotting. The remaining four to six animals per group were perfused with the fixatives of 4 % paraformaldehyde (Sigma) in phosphate-buffered saline (PBS). The brains were postfixed for more than 16 h in the same fixatives, cryoprotected in 30 % sucrose solution for 36–48 h and then stored at −80 °C. Frozen brains were sectioned into 20 µm by cryostat (3050S, Leica,

Germany) for immunohistochemical analysis with the indicated antibodies.

Dopamine measurement by HPLC

The dopamine content of various brain regions of mice was measured by HPLC with an electrochemical detection system. Briefly, the HPLC system consists of a solvent delivery system with an auto-sampler and electrochemical flow cell (VT-03, Antec, Leyden, The Netherlands). The mobile phase (100 mM $NaH_2PO_4 \cdot H_2O$, 0.74 mM heptane-1-sulfonic acid sodium salt, 0.027 mM EDTA, 2 mM KCl, and 10 % methanol; adjusted pH to 3 with phosphoric acid) was filtered through a 0.22 μm membranes filter (Critical, Inc.), degased for 30 min, and then pumped into the separation system of a C18 column (250 × 4.6 mm, Grace Alltima) at a flow rate of 0.8 ml/min. Brain tissues were extracted on ice with perchloric acid containing 0.45 mM sodium hydrosulfite. After sonication, lysates were centrifuged at 15,000×*g* for 10 min at 4 °C, and filtered through syringe with 0.22 μm nylon filters (Millipore). For ST-r, ST-m, ST-c, and NAc, 20 μl of lysate was injected for twice by auto-sampler. For CTX-m and VMB, single injection of 40 μl lysates was measured. Tissues were homogenized and lysates were collected immediately before measurement. To create the standard curve, the pure compounds of dopamine, 3,4-dihydroxyphenylacetic acid (DOPAC) and homovanillic acid (HVA) (Sigma, USA) were dissolved in lysis buffer at 20, 100, and 500 ng/ml (Fig. 2b). Integrated areas of the peaks were analyzed by software-based calculation (Clarity, DataApex) and normalized with the results of WT control mice.

Real-time qRT-PCR

Tissues were lysed in Trizol® (Invitrogen) followed by RNA extraction with the RNA-eazy purification kit (Qiagen). One microgram RNA was used for cDNA synthesis with SuperScript II reverse transcriptase (Invitrogen). Primers for tyrosine hydroxylase (*Th*), dopamine D1 receptor (*Drd1*), dopamine D2 receptor (*Drd2*), μ-opioid receptor (*Mor1*), calbindin-D28K (*CB*), hypoxanthine-guanine phosphoribosyl-transferase (*Hprt*), and interleukin-1 receptor-associated kinase 1 (*Irak1*) were designed by Primer 3 software (Table 1) and their specificity was confirmed by Primer-BLAST alignment. Real-time qPCR was performed in triplicate with the SYBR® Green PCR master mix (Applied Biosystems) in the Mx3000P real-time PCR system (Strategene). The mRNA levels of *Hprt* and *Irak1* gene were measured as the internal control and positive control, respectively. The expression levels of *Th*, *Drd1*, *Drd2*, *Mor1*, and *CB* were normalized with *Hprt* expression, and the normalized mRNA levels in *Mecp2* null mice were presented as the percentage of WT controls (% of WT).

Western blotting

Brain tissues were homogenized by sonication in lysis buffer containing protease inhibitors (Amresco). Twenty micrograms of protein lysate was separated by polyacrylamide gel electrophoresis (10 %, Bio-Rad) with 150 V for 1.5 h and transferred to a PVDF membrane (Millipore) by liquid electroblotting (Mini Trans-Blot Cell, Bio-Rad) with 350 mA for 1 h. The membrane was blocked by skim milk and incubated with primary (1:1,000, Millipore) or mouse anti-ß actin (1:100,000, Novus) at 4 °C for 16 h. Following incubation with peroxidase-conjugated goat-anti-rabbit or goat-anti-mouse secondary antibodies at room temperature for 2 h, the expression of DRD2 or ß-actin was detected by an enhanced chemoluminescence reagent kit (ECL, Millipore) under a bioimage acquisition system (Xlite 200R, Avegene Life Science). After densitometry-based quantification by Image J (NIH software), the intensity of DRD2 expression was normalized with that of ß-actin and then was presented as "% of WT".

Immunohistochemistry

Immunohistochemistry was performed as previously described (Liao et al. 2008). Briefly, brain sections were pretreated with 0.1 M PBS containing 0.2 % Triton X-100, 3 % H_2O_2, and 10 % methanol for 10 min, and then blocked with 3 % normal goat serum in 0.1 M PBS. Sections were incubated with the primary antibodies against MOR1 (1:10,000, Millipore, AB5511), CB (1:500, Cell Signaling, Cat. #2173), TH (1:2,000, Millipore, AB152), and PV (1:2,000; Sigma, P3088). All the antibodies are rabbit polyclonal except PV, which is a mouse monoclonal antibody. After incubation with primary antibody at room temperature for 16 h, sections were washed and then incubated with secondary antibody of biotinylated goat-anti-rabbit or horse-anti-mouse IgG (1:500) in 0.1 M PBS containing 1 % normal goat serum or normal horse serum for 2 h at room temperature. Sections were incubated for 1.5 h with avidin–biotin-complex (Elite ABC kit, Vector) and immunoreactivities were detected with 0.02 % diaminobenzidine (DAB, Sigma) in the presence of 0.0002 % H_2O_2 and 0.08 % nickel ammoniosulfate. Brain sections from *Mecp2*$^{-/y}$ mice and their WT littermate mice were processed in parallel and color developed in DAB solution for exactly the same duration to compare their immunoreactivity. Photomicrographs were taken by an upright microscopic system (Imager D2, Zeiss, Germany) equipped with a CCD camera (ORCA-R2 C10600-10B, Hamamatsu, Japan).

Results

Impaired locomotion, motor coordination, and motor learning in *Mecp2* null mice

Motor dysfunction is a hallmark feature of RTT. A previous report described motor deficits in *Mecp2* null ($Mecp2^{-/y}$) mice through manual analysis of grip strength, wire hanging, and open field activity (Guy et al. 2001). To evaluate the motor function in a quantitative manner, we subjected *Mecp2* null mice to a software-based open field test and a modified accelerating rotarod task. We first measured $Mecp2^{-/y}$ male mice and their WT littermates with an open field test, at 4–5 weeks of age, which is prior to the onset of severe RTT-like symptoms. We found that $Mecp2^{-/y}$ mice traveled significantly shorter distances (83.9 ± 2.2 % of WT, $p < 0.001$) with longer immobility time (112.6 ± 3.3 % of WT, $p < 0.01$), lower average velocity (89.2 ± 1.7 % of WT, $p < 0.001$) and maximal velocity (69.7 ± 3.7 % of WT, $p < 0.001$) compared with their WT controls (Fig. 1a, b). These results indicate that lack of MeCP2 significantly impairs ambulatory ability in mice. $Mecp2^{-/y}$ mice also showed a significant thigmotaxis, a tendency to avoid the center arena (71.1 ± 12.3 % of WT, $p < 0.05$), indicating an elevated state of anxiety in *Mecp2* null mice (Fig. 1a, b) that is consistent with previous study in mice with forebrain-specific deletion of *Mecp2* (Gemelli et al. 2006).

To measure motor coordination and motor learning, we assessed the aforementioned cohorts of mice using an accelerated rotarod test over five consecutive days. Male $Mecp2^{-/y}$ mice showed significantly reduced latency to fall on the first day of testing compared with the WT mice [Falling latency (s): 17.9 ± 4.1 in KO vs. 69.0 ± 9.6 in WT, $p < 0.001$; Fig. 1c], indicating that motor coordination was impaired in the null mice. From testing day 2 to day 5, the $Mecp2^{-/y}$ mice demonstrated a flat learning curve compared with WT mice for acquisition of the motor skills: From day 1–3, the MLI [$MLI_n = (T_n - T_{n-1})/T_{n-1} \times 100$ %] was higher in $Mecp2^{-/y}$ mice than that of WT mice ($p < 0.05$; Fig. 1d). From day 3 to day 4, however, the MLI of $Mecp2^{-/y}$ mice was significantly lower compared with WT mice ($MLI_4 = 3.3 \pm 10.4$ % in KO vs. 44.9 ± 11.5 % in WT, $p < 0.05$; Fig. 1d), suggesting that motor skill learning is impaired following loss of MeCP2.

Given that RTT primarily affects females, the female heterozygous ($Mecp2^{+/-}$) littermates of male *Mecp2* null mice were tested in parallel. We did not find any significant locomotion deficits in females until 10–12 weeks of age (data not shown), indicating the delayed onset of motor symptoms in female *Mecp2* mutants. Moreover, the deficit in motor skill learning was also not found in female $Mecp2^{+/-}$ mice up until 10–12 weeks of age (Fig. 1e, f). The female $Mecp2^{+/-}$ mice showed a comparable falling latency to the WT control on the first testing day (20.4 ± 3.9 in $Mecp2^{+/-}$ vs. 32.5 ± 9.7 in WT, $p > 0.05$; Fig. 1e), but failed to learn the motor skills from day 3 to 4 ($MLI_4 = -15.3 \pm 7.7$ % in $Mecp2^{+/-}$ vs. 25.6 ± 13.1 % in WT, $p < 0.05$; Fig. 1f). These results were consistent with previous findings suggesting that female heterozygous mutants also develop RTT-like phenotypes but at a later developmental age compared with male *Mecp2* null mice. Given that *Mecp2* is an X-linked gene, which can be randomly inactivated in female individuals (Amir et al. 2000), we thus analyzed the striatal phenotypes in male *Mecp2* null mice in the rest of this study to avoid the mosaic expression of MeCP2 that may complicate the data interpretation.

Reduced dopamine content in the striatum of $Mecp2^{-/y}$ mice

Previous studies reported that the brains of both RTT patients and *Mecp2* mutant mice contain reduced level of dopamine (Dunn et al. 2002; Samaco et al. 2009; Panayotis et al. 2011; Gantz et al. 2011). Given that the dopaminergic projections from the substantia nigra (SN) topographically innervate the striatum along the rostral–caudal axis (Hontanilla et al. 1996), we systemically analyzed the dopamine content in the rostral, middle and caudal striatum as well as other related brain areas from $Mecp2^{-/y}$ or WT control mice (Fig. 2a). We found that the dopamine levels in $Mecp2^{-/y}$ mice was significantly reduced in the dorsal striatum (caudate putamen) across the rostral–caudal axis, with a 62 % reduction in the rostral striatum (ST-r, 38.0 ± 11.2 % of WT, $p < 0.001$, $n = 6$) and a modest reduction (~20 %) in the middle and caudal striatum (ST-m and ST-c, $n = 6$) (Fig. 2c, d). The dopamine content was also significantly reduced in the NAc (34.2 ± 2.3 % of WT, $p < 0.001$, $n = 5$; Fig. 2d), which is the ventral striatum at the rostral forebrain receiving dopaminergic inputs from the mesolimbic pathway. The VMB, where the majority of dopaminergic neurons are located, also contained lower dopamine levels in $Mecp2^{-/y}$ mice (42.9 ± 8.1 % of WT, $p < 0.001$, $n = 4$) (Fig. 2d). In contrast, the dopamine level was not affected in the cerebral cortex at middle level (CTX-m, which is a non-dopaminergic projection area) in $Mecp2^{-/y}$ mice (92.2 ± 16.1 % of WT, $p > 0.05$, $n = 4$; Fig. 2d). These results demonstrate that loss of MeCP2 significantly altered the dopamine content in the striatum, particularly in the rostral striatum.

Given that dopamine levels were measured from tissue homogenates containing both presynaptic and postsynaptic compartments, the reduction of dopamine in the striatum could be due to a reduction in dopaminergic innervations, reduced biosynthesis of dopamine or reduced release at the

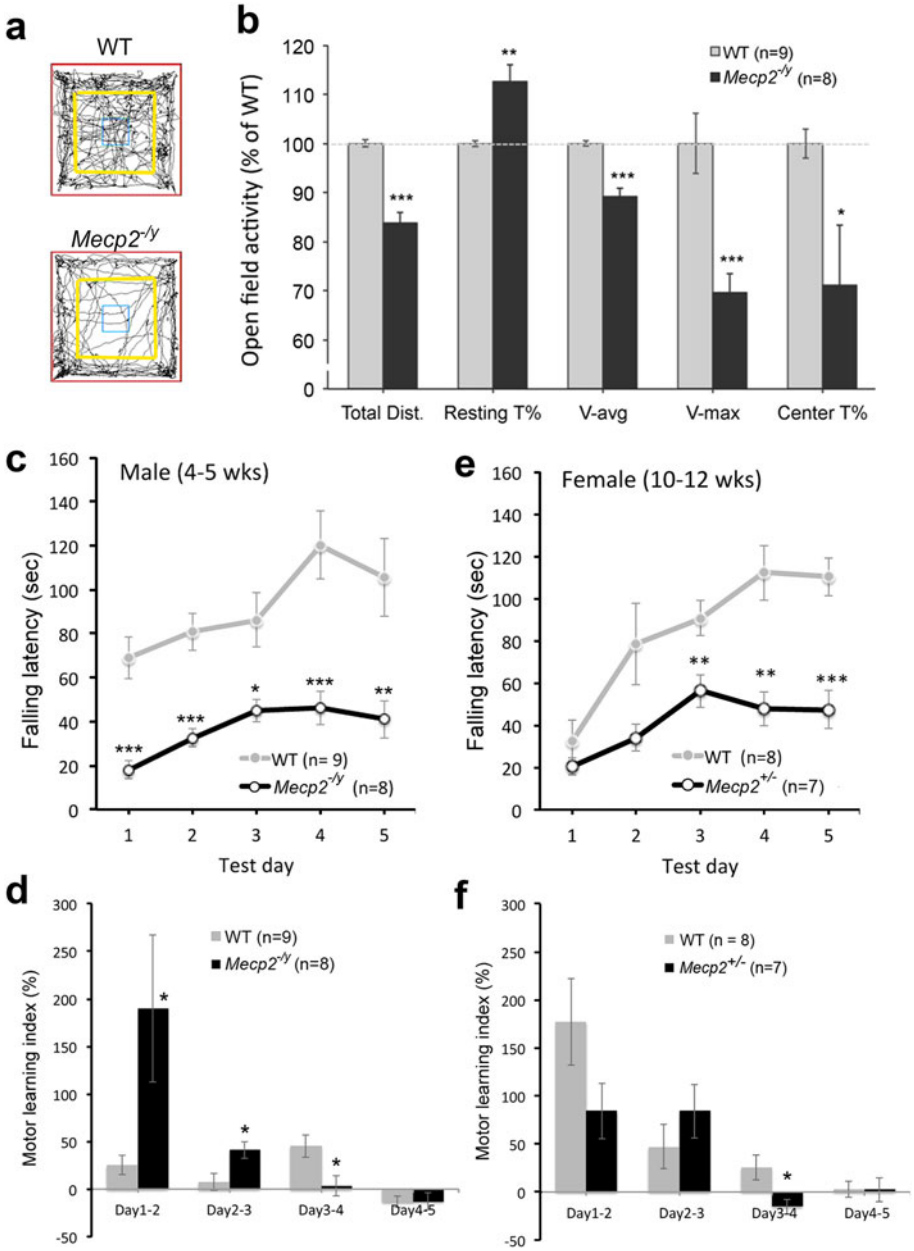

Fig. 1 Locomotor activity and motor skill learning in *Mecp2*$^{-/y}$ and wild-type mice. *Mecp2*$^{-/y}$ mice show hypoactivity in an open-field test. The male mice at 4–5 weeks of age were tested for 16 min and the video footage of the last 12 min was analyzed. The exploration trajectories (**a**) and software-based locomotion analysis (**b**) show that *Mecp2*$^{-/y}$ mice travel shorter distance with lower velocity and take more rest compared with wild-type (WT) mice. These *Mecp2*$^{-/y}$ mice also spend less time crossing the center arena [the area inside the *yellow square* (**a**)]. The mutant mice and their WT controls were then tested on an accelerating rotarod for three trials a day over five consecutive days. The median scores of daily trials were used for statistical analysis. The male mutants showed a significant impairment of motor coordination in the first test day (**c**). Both male (**c**, **d**) and older female mutants (**e**, **f**) showed deficits in the late phase (day 3–4) of motor skill learning. **d**, **f** The "motor learning index" represents the percentage of learned skills between 2 days. Data are expressed as mean ± SEM. $*p < 0.05$, $**p < 0.01$, $***p < 0.001$, compared with WT littermate controls; paired Student *t* test for **a**, **b**, **d**, **f** and two-way ANOVA followed by post hoc Bonferroni test for **c** and **e**. *Total Dist*, total traveled distance; *Resting T %*, percent of time at resting; *V-avg*, average velocity of locomotion (excluding the resting time); *V-max*, maximal velocity of locomotion; *Center T %*, percent of time crossing the center arena

dopaminergic terminals. Panayotis et al. (2011) demonstrated that the number of neurons expressing TH (the rate-limiting enzyme responsible for the biosynthesis of dopamine) is decreased in the SN. To examine whether loss of MeCP2 affects expression of TH and dopamine signaling molecules, we examined the mRNA levels of *Th* and

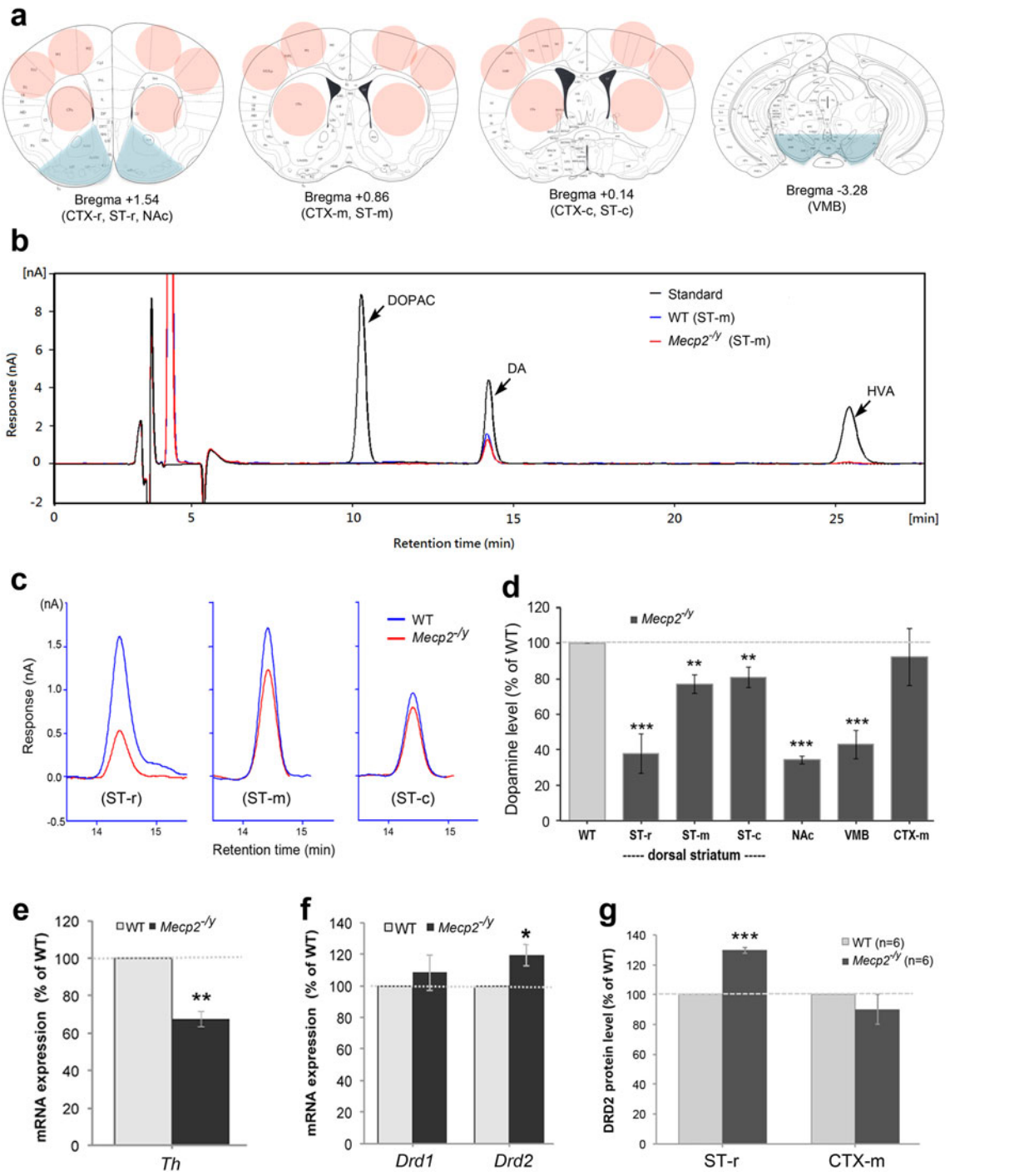

Fig. 2 Dopaminergic transmission in selective brain regions of *Mecp2*$^{-/y}$ and WT mice. **a** Maps of mouse brain show that tissues from different brain regions were harvested manually (*blue shadows*) or by tissue punch (*pink circles*) from male mice at 4–5 weeks of age. **b** Dopamine and its metabolites were measured by HPLC. The superimposed measurements of standards (DOPAC, dopamine and HVA) and tissue homogenates from the middle striatum (ST-m) indicate the absence of dopamine metabolites in our tissues. **c** Representative traces of dopamine measurements in different subregions of the striatum in *Mecp2*$^{-/y}$ and WT mice. **d** An approximately 60 % reduction of dopamine in the rostral striatum (ST-r), nucleus accumbens (NAc) and ventral midbrain (VMB) is shown in *Mecp2*$^{-/y}$ mice compared with WT mice ($n = 6$). There was no significant change found in the middle level of cerebral cortex (CTX-m). *Mecp2*$^{-/y}$ mice exhibit reduced expression of tyrosine hydroxylase (*Th*, in **e**) and increased dopamine D2 receptor (*Drd2*, in **f**) in the ST-r as examined by qRT-PCR ($n = 4$). **g** Immunoblotting shows increased DRD2 protein in the ST-r but not in the CTX-m of *Mecp2*$^{-/y}$ mice ($n = 6$). Data are expressed as mean ± SEM. $^{*}p < 0.05$, $^{**}p < 0.01$, $^{***}p < 0.001$, compared with WT by Student *t* test. *DA*, dopamine; *DOPAC*, 3,4-dihydroxyphenylacetic acid; *Drd1*, dopamine D1 receptors; *HVA*, homovanillic acid; *ST-c*, caudal striatum

dopamine receptors including dopamine D1 receptor (*Drd1*) and dopamine D2 receptor (*Drd2*) in the striatum of *Mecp2*$^{-/y}$ mice and their WT controls. We found that *Mecp2*$^{-/y}$ mice showed a reduction in *Th* (61.7 ± 5.8 % of WT, $p < 0.01$, $n = 4$; Fig. 2e) and an increase in *Drd2* (119.9 ± 8.7 % of WT, $p < 0.05$, $n = 4$; Fig. 2f) expression in the rostral striatum, without significant alteration in *Drd*1 expression compared with the WT controls (106.4 ± 16.2 % of WT, $p > 0.05$, $n = 4$; Fig. 2f). The protein expression of DRD2 was significantly increased in the rostral striatum (129.6 ± 2.0 % of WT, $p < 0.001$, $n = 6$; Fig. 2g), but not in the cortex of *Mecp2*$^{-/y}$ mice compared with the WT controls (90.1 ± 9.9 % of WT, $p > 0.05$, $n = 6$; Fig. 2g). The protein level of TH was also not altered in cortical tissues of *Mecp2*$^{-/y}$ mice compared to WT controls (96.5 ± 36.1 % of WT, $p > 0.05$, $n = 6$), suggesting that the down-regulation of *Th* gene expression is specific to the striatum. Notably, a comparable reduction of *Th* mRNA was observed in the striatum of female *Mecp2*$^{+/-}$ mice at 10–15 weeks of age (73.0 ± 2.4 % of WT, $p < 0.05$, $n = 4$) and we also found a significant decrease of dopamine content in the striatum of *Mecp2*$^{+/-}$ females (ST-r: 80.3 ± 4.0 % of WT, $p < 0.01$; $n = 5$). These results suggest that the striatal MeCP2 is required to maintain appropriate striatal levels of dopamine and serve as a critical regulator of the striatal genes involved in dopamine signaling.

Location-dependent reduction of MOR1 expression in the striatum of *Mecp2*$^{-/y}$ mice

The differential reduction of dopamine in the rostral–caudal striatum in *Mecp2*$^{-/y}$ mice indicates that MeCP2 modulates striatal dopamine content in a subregion-specific manner. However, there is not a corresponding rostral–caudal gradient in TH protein expression (unpublished observation), suggesting other region-specific molecules in the striatum may render this rostral–caudal modulation of dopamine. Previous studies have demonstrated that the striatum is anatomically different along the rostral–caudal axis with the "striosomes" being enriched within the rostral striatum. The striosomes are also named "patches" or "dopamine islands" (Graybiel 1984) containing abundant nerve terminals expressing the μ-opioid receptor 1 (MOR1) (Herkenham and Pert 1981). Given that activation of MOR1 is known to regulate dopamine release (Di and Imperato 1988; Piepponen et al. 1999) and MOR1 is one of the target genes for MeCP2-mediated transcriptional regulation (Hwang et al. 2009), we tested whether loss of MeCP2 could alter MOR1 expression in striosomes in a differential pattern along the rostral–caudal axis of the striatum.

We found that *Mor1* mRNA expression was significantly down-regulated in the rostral striatum of *Mecp2*$^{-/y}$ mice compared with WT controls (55.3 ± 6.6 % of WT, $p < 0.05$, $n = 4$), while the expression of matrix-associated *CB* mRNA was not significantly affected (93.5 ± 8.1 % of WT, $p > 0.05$, $n = 4$; Fig. 3a). The down-regulation of *Mor1* in the rostral striatum of *Mecp2*$^{-/y}$ mice was also observed at the protein level as the area of MOR1-immunoreactive (MOR1^{+}) patches was significantly reduced in the mutants compared with WT mice (Fig. 3b, b', d, d'). Quantification of MOR1^{+} areas with a constant threshold of mean density showed that the reduction of MOR1^{+} area was primarily located within the rostral striatum (59.2 ± 7.4 % of WT, $p < 0.05$, $n = 3$), but there was no difference in the middle and caudal striatum ($p > 0.05$; Fig. 3c). Notably, the reduction of MOR1^{+} areas was not caused by loss of striosomal neurons since the zones lacking CB expression (arrowheads in Fig. 4a–b') were preserved in the rostral striatum of *Mecp2*$^{-/y}$ mice. MOR1 protein expression also remained unchanged in other brain areas such as the thalamus and hypothalamus in *Mecp2*$^{-/y}$ mice (Fig. 3e, e'; unpublished observations). These results demonstrated that MeCP2 could positively regulate MOR1 expression in a striosome-specific manner.

Increased number of calbindin-positive neurons in the striatum of *Mecp2*$^{-/y}$ mice

To further examine whether loss of MeCP2 affects the striatal matrix compartment that is enriched with projection neurons expressing CB (Liu and Graybiel 1992), we examined the expression of CB in the striatum along the rostral–caudal axis. In WT mice, we found that the CB^{+} neurons were heterogeneously distributed in the matrix compartment with a decreasing gradient from ventromedial to dorsolateral striatum (dlST) (Fig. 4a, b). By counting the number of CB^{+} neurons in a square of 250 μm^2 throughout different locations of the striatum (inset in Fig. 4e) from rostral to caudal levels, we found that only a limited number of CB^{+} neurons were located in the dorsomedial striatum (dmST) and dlST of WT mice (Fig. 4a, c, e, f). A significant increase in the number of CB^{+} neurons was observed in the dlST from rostral to caudal levels of *Mecp2*$^{-/y}$ mice ($p < 0.05$; Fig. 4a', c', f); however, there was no difference in the dmST ($p > 0.05$; Fig. 4e). We also observed a significant increase in the number of CB^{+} neurons in the ventromedial striatum (vmST) ($p < 0.05$; Fig. 4b', d' compared with b, d; Fig. 4g, i) and in the ventrolateral striatum (vlST) throughout the rostral–caudal axis in *Mecp2*$^{-/y}$ mice ($p < 0.05$; Fig. 4h, i). These data indicate that the number of CB^{+} matrix neurons is increased in the absence of MeCP2, which is opposite to the reduction of MOR1 expression observed in the striosomal compartment.

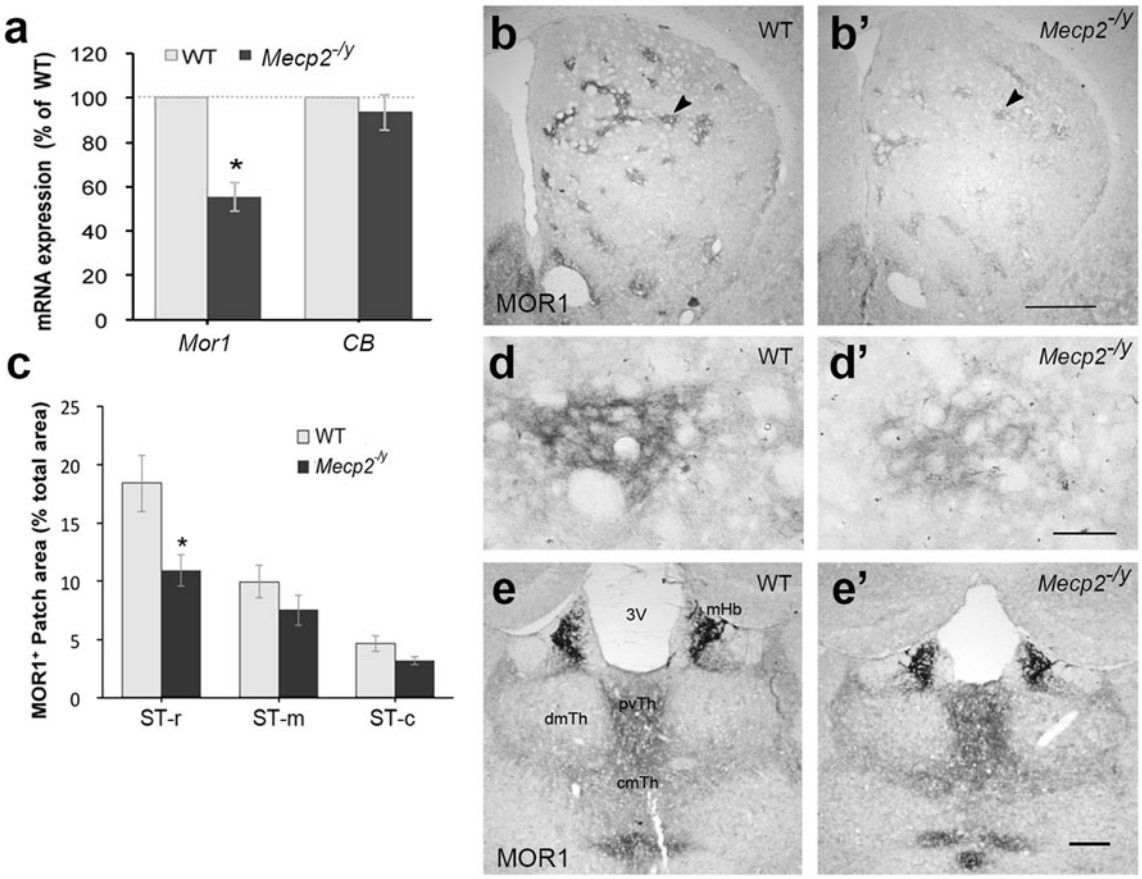

Fig. 3 MOR1 expression in the striosomes of the striatum. **a** Transcripts of μ-opioid receptors (*Mor1*) and calbindin (*CB*) were measured in the rostral striatum (ST-r) from *Mecp2*$^{-/y}$ mice or WT littermate controls by qRT-PCR ($n = 4$ pairs). *Mecp2*$^{-/y}$ mice show a significant reduction in *Mor1* expression. **b–d'** Protein expression of MOR1 in striosomes (*arrowheads*) is reduced by 40 % in the ST-r of *Mecp2*$^{-/y}$ mice ($n = 4$ pairs). High power images of the striosomes in **b** and **b'** (*arrowheads*) are shown in **d** and **d'**, respectively. **e**, **e'** MOR1 protein expression is unaltered in the thalamic area of *Mecp2*$^{-/y}$ mice. *Scale bar* in **b'** (for **b**, **b'**), 500 μm; in **d'** (for **d**, **d'**), 50 μm; in **e'** (for **e**, **e'**), 200 μm. Data are expressed as mean ± SEM. *$p < 0.05$, compared with WT by student *t* test. *cmTh*, centromedial thalamic nucleus; *dmTh*, dorsomedial thalamic nucleus; *mHb*, medial habenular nucleus; *pvTh*, paraventricular thalamic nucleus; *ST-m*, middle striatum; *ST-c*, caudal striatum; *3V*, third ventricle

Increased number of parvalbumin-positive interneurons in the striatum of *Mecp2*$^{-/y}$ mice

Given that striatal motor output is modulated by the activity of GABAergic interneurons such as the fast-spiking PV$^+$ interneurons (Kreitzer and Malenka 2008), and depletion of dopamine alters PV$^+$ inhibitory microcircuits in the striatum (Gittis et al. 2011), it is possible that loss of MeCP2 reduces dopamine content leading to alterations of PV$^+$ interneurons in the striatum. To test this possibility, we examined the expression of PV in the striatum of *Mecp2*$^{-/y}$ mice using immunostaining.

We found that PV$^+$ interneurons are distributed in a decreasing gradient of dorsal-to-ventral and lateral-to-medial part in the striatum of WT mice (Fig. 5a, b), consistent with previous findings (Wu and Parent 2000). Upon quantification of the number of PV$^+$ interneurons, we found that the total number of PV$^+$ cells was significantly increased throughout the striatum of *Mecp2*$^{-/y}$ mice with the strongest augmentation in the rostral striatum (186.9 ± 18.7 % of WT, $p < 0.01$, $n = 5$; Fig. 5a, a', e). Notably, the number of PV$^+$ interneurons was increased more than twofold in the dmST throughout the rostral–caudal axis (dmST-r: 262.3 ± 35.1 % of WT, $p < 0.01$; dmST-m: 207.7 ± 26.2 % of WT, $p < 0.01$; dmST-c: 251.8 ± 23.0 % of WT, $p < 0.001$; $n = 5$; Fig. 5f) and over threefold in the NAc (342.9 ± 5.5 % of WT, $p < 0.001$; $n = 3$; Fig. 5h) in *Mecp2*$^{-/y}$ mice. A mild but significant increase of PV$^+$ neurons was also found in the dlST only at the rostral level (dlST-r: 139.1 ± 15.0 % of WT, $p < 0.05$; dlST-m: 127.8 ± 10.4 % of WT, $p > 0.05$; dlST-c: 144.7 ± 20.5 % of WT, $p > 0.05$; $n = 5$; Fig. 5g) and in the cerebral cortex (CTX, specifically in the area of cingulate cortex) at the rostral and middle level (CTX-r: 116.9 ± 2.6 % of WT, $p < 0.05$; CTX-m: 120.2 ± 6.3 % of WT, $p < 0.05$; CTX-c: 131.3 ± 20.9 % of WT,

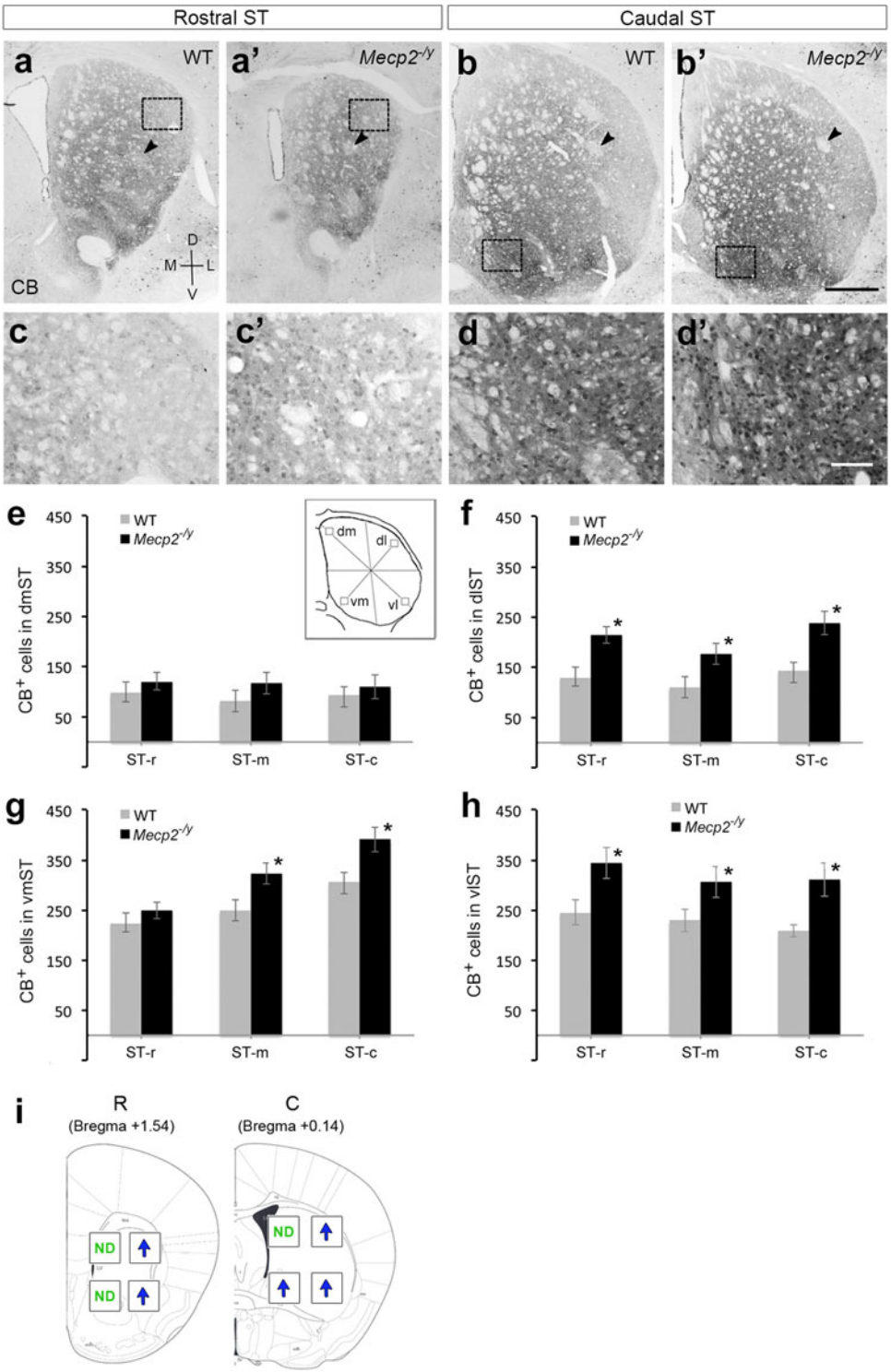

Fig. 4 Calbindin-expressing neurons in the matrix compartment of the striatum. Increased calbindin-positive (CB^+) neurons are shown in the dorsolateral striatum (dlST; **a**, **a'**) and ventromedial striatum (vmST; **b**, **b'**) at the rostral (**a**, **a'**) and caudal (**b**, **b'**) levels of the striatum in male mice at 4- to 5-week of age. *Arrowheads* in **a**–**b'** indicate the CB-poor zones (the striosomes). High-power images of the *boxed areas* in **a**–**b'** are shown in **c**–**d'**, respectively. Quantification of CB^+ neurons in different subregions of the striatum (*inset* in **e**). *Mecp2*$^{-/y}$ mice exhibit an increase in the number of CB^+ neurons in the dlST (**f**), vmST (**g**) and ventrolateral striatum (vlST, **h**), but not in the dorsomedial striatum (dmST, **e**) ($n = 5$ pairs). **i** Summary of increased CB^+ neurons in the striatum of *Mecp2*$^{-/y}$ mice. *Blue arrows*, moderate increase; *ND*, no difference. *Scale bar* in **b'** (for **a**–**b'**), 500 μm; in **d'** (for **c**–**d'**), 50 μm. Data are expressed as mean ± SEM. *$p < 0.05$, compared with WT by Student *t* test. *ST-r*, rostral striatum; *ST-m*, middle striatum; *ST-c*, caudal striatum; *R*, rostral level; *C*, caudal level

$p > 0.05$; $n = 5$; Fig. 5i) in *Mecp2*$^{-/y}$ mice. We also observed that the dendritic arborization of the PV^+ interneurons was significantly extended in the dmST and dlST of *Mecp2*$^{-/y}$ mice compared with WT controls (Fig. 5d, d'). These findings suggest that MeCP2 may control the number of PV^+ interneurons and their dendritic arborization within the striatum in vivo.

Discussion

In the present study, we characterized the molecular and cellular phenotypes in the striatum of *Mecp2* null mice. We found that *Mecp2* null mice showed impaired locomotion and motor skill learning, which was accompanied by a dramatic reduction of dopamine content in the

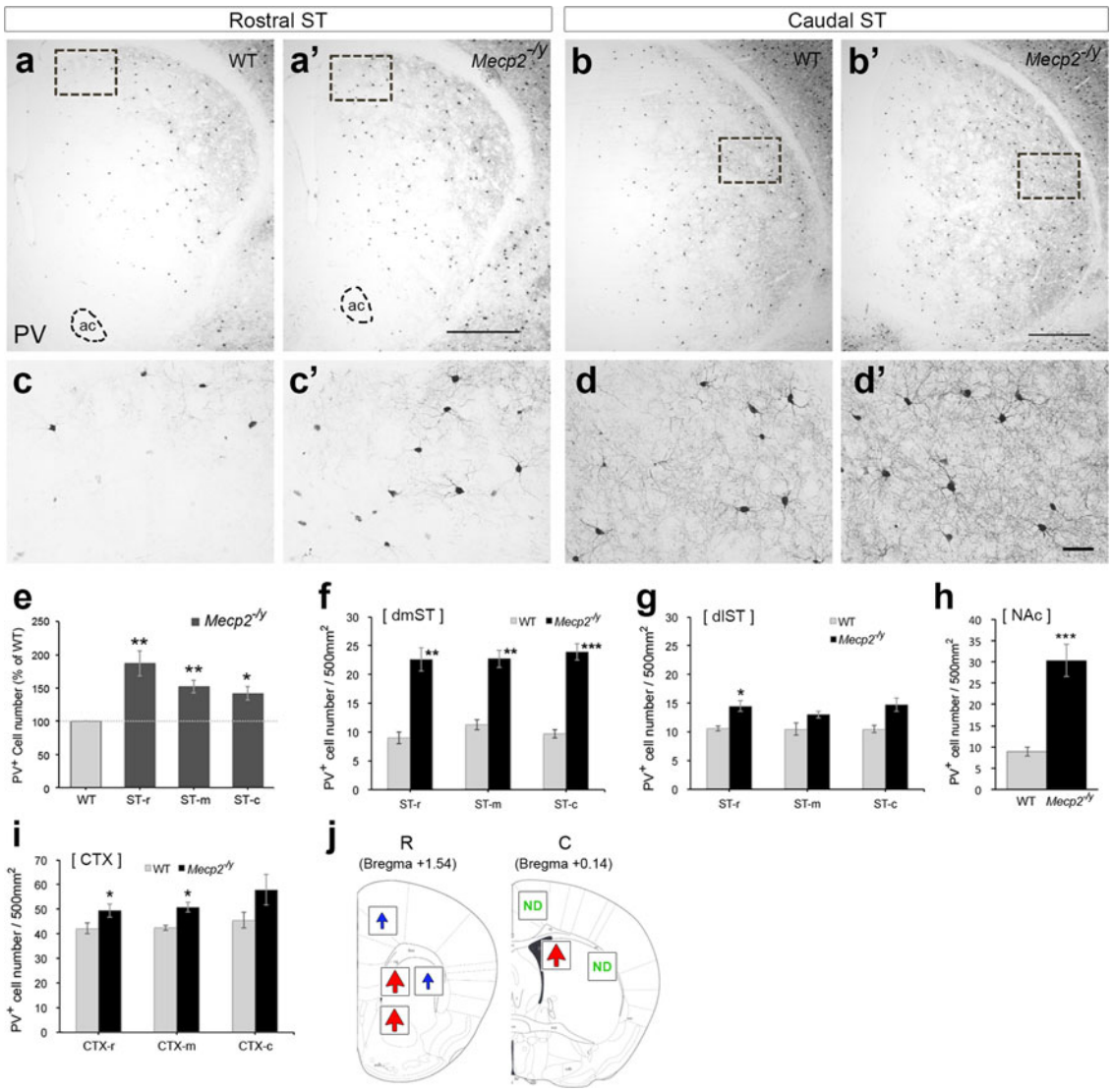

Fig. 5 Parvalbumin-positive interneurons in the striatum of *Mecp2*$^{-/y}$ and WT mice. Parvalbumin (PV) was examined in brain sections from *Mecp2*$^{-/y}$ and WT mice at 4–5 weeks of age by immunohistochemistry. PV-positive (PV^{+}) neurons in the striatum along the rostral (**a**, **a'**) to caudal (**b**, **b'**) axis. High power images of the *boxed areas* in **a–b'** are shown in **c–d'**. The PV^{+} neurons of *Mecp2*$^{-/y}$ mice develop more extensive dendritic arborization compared with WT mice. **e** Total number of PV^{+} neurons in the striatum of *Mecp2*$^{-/y}$ mice was quantified at different rostral–caudal positions and normalized with PV^{+} cell number in WT littermate controls ($n = 5$ pairs). Robust enhancement of the number of PV^{+} neurons is distributed in the dorsomedial striatum (dmST, **f**) and nucleus accumbens (NAc, **h**), whereas moderate increase of PV^{+} neurons occurs in the rostral part of dorsolateral striatum (dlST, **g**) and the rostral/middle levels of the cerebral cortex (CTX, **i**) ($n = 5$ pairs). **j** Summary of increased PV^{+} neurons in the striatal and cortical areas of *Mecp2*$^{-/y}$ mice. *Red arrows*, robust increase; *blue arrows*, moderate increase; *ND*, no difference. *Scale bar* in **a'** (for **a**, **a'**) and **b'** (for **b**, **b'**), 500 μm; in **d'** (for **c–d'**), 50 μm. Data are expressed as mean ± SEM. $*p < 0.05$, $**p < 0.01$, $***p < 0.001$, compared with WT by Student *t* test. *ac*, anterior commissure; *ST-r*, rostral striatum; *ST-m*, middle striatum; *ST-c*, caudal striatum; *R*, rostral levels; *C*, caudal level

rostral striatum. Moreover, loss of MeCP2 disrupts the expression of multiple genes involved in dopamine signaling (i.e., *Th* and *Drd2*) and striatal compartmentalization (i.e., *Mor1* and *CB*), and significantly increases the number of PV^{+}-inhibitory neurons and their dendritic arborization in the striatum. These alterations were found predominantly in the rostral striatum, suggesting a regional selectivity of MeCP2-mediated modulation of striatal gene expression. Together, our findings suggest that MeCP2 plays a critical role in psychomotor control by maintaining normal striatal dopamine signaling, a balanced neurochemistry in the striosome/matrix, and an appropriate number and dendritic complexity of inhibitory interneurons in the striatum. Loss of MeCP2 disrupts the striatal structure and function, those may underlie the motor deficits in RTT.

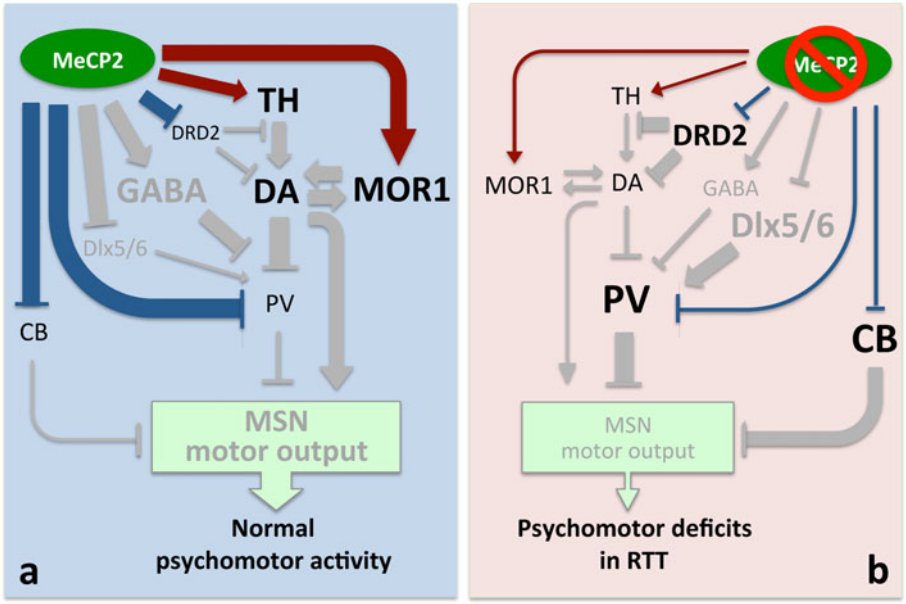

Fig. 6 Putative model for MeCP2-dependent regulation of striatal genes associated with psychomotor deficits in RTT. **a** MeCP2 regulates a set of genes in the striatum in a direct or indirect manner. **b** In the absence of MeCP2, reduced dopamine levels and enhanced DRD2 and PV/CB in the striatum may activate the indirect pathway and diminish the motor outputs from MSNs, leading to psychomotor deficits in RTT. *Arrows* or *flat-arrows* indicate positive or negative regulation, respectively, with their relative effectiveness indicated by thickness. *Letter size* corresponds to expression level. *Letters and arrows/flat arrows in gray* indicate the molecular links reported in the literatures. *CB*, calbindin; *DRD2*, dopamine D2 receptor; *DA*, dopamine; D*lx5/6*, distal-less homeobox 5/6; *GABA*, γ-amino butyric acid; *MeCP2*, methyl CpG binding protein 2; *MOR1*, μ-opioid receptor 1; *MSN*, median spiny neuron; *PV*, parvalbumin; *TH*, tyrosine hydroxylase. See text for details

MeCP2-mediated regulation of dopamine in the striatum

In the present study, we found that dopamine content was reduced in both the striatum (ST-r, ST-m, ST-c, and NAc) and VMB (SN and ventral tegmental area) in *Mecp2*$^{-/y}$ mice (Fig. 2d). The reduction of dopamine is accompanied by decreased *Th* expression in the striatum and VMB (this study and Panayotis et al. 2011), suggesting that loss of MeCP2 may diminish dopamine synthesis both in the soma and terminals of the dopaminergic neurons. Notably, we found that expression of *Drd2* is increased in the striatum of *Mecp2*$^{-/y}$ mice (Fig. 2f, g), which is consistent with previous studies showing that dopamine binding to DRD2 is increased in the striatum of RTT patients (Chiron et al. 1993; Dunn et al. 2002). Despite of the fact that DRD2 is a presynaptic autoreceptor that inhibits release of dopamine (Ungerstedt et al. 1985), recent evidence suggests that postsynaptic DRD2 on the striatal neurons can also affect dopamine release by modulating the activity of local striatal circuits via the indirect pathway (Anzalone et al. 2012). Therefore, up-regulation of DRD2 may lead to reduction in dopamine release following neuronal activation in the striatum of *Mecp2* null mice.

On the other hand, activation of DRD2 can selectively inhibit the phosphorylation of TH at Ser40, leading to reduced synthesis of dopamine in the striatum (Lindgren et al. 2001). Consistently, Ser40 phosphorylation of the TH protein is significantly reduced in the SN and the striatum of *Mecp2* null mice (Panayotis et al. 2011). Here, we reasoned that MeCP2 may maintain striatal dopamine content by repressing DRD2 expression in the striatum (Fig. 6a). De-repression of DRD2 in *Mecp2*$^{-/y}$ mice may reduce striatal dopamine content by inactivation of TH in the striatum (Fig. 6b). Notably, a recent finding shows that re-expressing *Mecp2* specifically into TH^{+} neurons can only partly rescue the motor deficits in MeCP2-deficient mice (Lang et al. 2013), supporting the notion that MeCP2 in neurons other than catecholaminergic neurons, such as the GABAergic neurons, may also play an essential role in motor control.

MeCP2-mediated gene regulation in the striatum

μ-Opioid receptor 1 (MOR1)

In the absence of MeCP2, we observed a reduction in the area of MOR1^{+} striosomes and an increase in the number of CB^{+} matrix neurons. The reduction of MOR1^{+} areas in the striatum of *Mecp2*$^{-/y}$ mice (Fig. 3) is unlikely to be due to cell loss of striosomal neurons because the CB-negative zones in the striatum of adjacent sections were preserved.

Given that MeCP2 is a transcriptional regulator, it is possible that MeCP2 directly regulates MOR1 expression. Previous reports have demonstrated that MeCP2 negatively regulates MOR1 expression at the transcriptional level (Hwang et al. 2009; Samaco et al. 2012). Our findings that MOR1 protein is selectively reduced in the striosomes compared with other brain areas (e.g., the medial habenula) in *Mecp2* null mice suggest that MeCP2 may positively regulate MOR1 expression in a region- and cell type-specific manner. In addition to the MeCP2-mediated direct transcriptional regulation of MOR1, the innervation of dopamine-containing fibers is required for the expression of striosomal markers, including MOR1 (van der Kooy and Fishell 1992). Thus, the reduction of MOR1 expression in the striosomes of mice lacking MeCP2 may also be a result of reduced dopamine innervation to the striosomes during early postnatal development.

The down-regulation of MOR1 in the striosomes may affect psychomotor control of the striatum. Previously, the activation of MOR1 was shown to enhance dopamine transmission through inhibition of GABAergic activities (Johnson and North 1992), and the MOR1-mediated GABAergic inhibition selectively occurs in the striosomal compartment (Miura et al. 2007). Here, we have observed a reduction of MOR1 expression in the striosomes, which may result in a decrease of dopamine signaling in the striatum of *Mecp2* null mice (Fig. 6b), indicating that pharmacological enhancement of MOR1 activity in the striatum may restore striatal dopamine transmission and improve motor function in the MeCP2-deficient mice. The MOR1-positive striosomal cells have been implicated in maternal/social attachment behavior, motor stereotypy, and motor skill learning (Canales and Graybiel 2000; Moles et al. 2004; Lawhorn et al. 2009; Burkett et al. 2011). Our findings therefore suggest that MOR1 is likely to be a key molecule associated with stereotypic hand wringing and motor learning deficits observed in RTT.

Calbindin-D28K (CB)

In the present study, we observed an increase in CB^+ neurons in the DL-ST of *Mecp2*$^{-/y}$ mice (Fig. 4). The increase in CB^+ neurons is not likely to be due to the increased number of matrix neurons because the striatal volume is smaller in RTT patients or *Mecp2*-null mice compared with normal persons or WT mice (Reiss et al. 1993; Dunn et al. 2002; Stearns et al. 2007), and we did not observe a change in cell density in the striatum as counted by Nissl staining in *Mecp2* null mice (unpublished observation). Because the mRNA level of *CB* was not changed (Fig. 3a), the increase of CB^+ neurons in the striatum of *Mecp2* null mice (Fig. 4) may result from up-regulation of protein synthesis of CB in the matrix neurons. Previous studies have reported that the *CB* mRNA can be post-transcriptionally regulated at the 3′-untranslated region (UTR), which is frequently targeted by miRNAs for translational suppression (Enomoto et al. 1992; Barmack et al. 2010). In light of a recent finding that loss of MeCP2 dysregulates the transcription of multiple miRNAs (Szulwach et al. 2010), the up-regulation of CB protein expression in matrix neurons could be a result of translational de-repression by MeCP2-regulated miRNAs. In addition to direct regulation by MeCP2, expression of CB can also be positively regulated by DRD2 in the matrix neurons (Jung et al. 2000), suggesting that the increase in CB in the striatum of *Mecp2* null mice may indirectly consequence of up-regulated DRD2.

Calbindin-D28K is a calcium-binding protein involved in neuronal protection by buffering intracellular calcium (Figueredo-Cardenas et al. 1998; Yenari et al. 2001). An increase in cytosolic CB in neurons was reported to lower the probability of exocytosis and reduce neurotransmitter release (Pan and Ryan 2012), suggesting that a reduced output from the neurons in the striatal matrix may lead to motor deficits in *Mecp2*$^{-/y}$ mice. Moreover, CB also functions as a sensor and transporter of synaptic calcium, playing a non-canonical role in fine-tuning synaptic plasticity and calcium dynamics (Schmidt 2012). Manipulating the level of CB in hippocampal neurons by a gain or loss of function impairs the induction of LTP and long-term spatial memory (Jouvenceau et al. 2002; Dumas et al. 2004), suggesting the importance of CB in cognitive function. In the present study, we found a MeCP2-mediated suppression of CB in the dlST but not the dmST in the dorsal striatum (Fig. 4). The dlST is the primary sub-region of the striatum that receives dopaminergic innervation from the SNpc (Moore et al. 2001) and has been implicated in sensorimotor loop of learning and the late phase of habit formation (Yin et al. 2009; Thorn et al. 2010; Hilario et al. 2012). Enhanced CB expression in the matrix neurons of dlST in *Mecp2*$^{-/y}$ mice suggests that loss of MeCP2 may impede synaptic transmission and plasticity of the matrix neurons in the dlST and cause deficits in the late phase of motor skill learning and habit formation (Fig. 6b), which is consistent with our observation of a reduction in MLI in *Mecp2*$^{-/y}$ mice (Fig. 1d, f).

Parvalbumin (PV)

In the present study, we found an increase in the number and enhanced dendritic arborization of PV^+ interneurons in the striatum of *Mecp2* null mice (Fig. 5). The enhanced number of PV^+ neurons in *Mecp2*$^{-/y}$ mice might be due to de-repression of PV gene by loss of MeCP2 (Fig. 6b). In support of this, previous microarray study suggest that loss of MeCP2 up-regulates PV mRNA, while mice over-

expressing MeCP2 show reduced PV expression (Chahrour et al. 2008). Alternatively, MeCP2 may control PV expression indirectly by regulating the Dlx5/6 transcription factor, which specifies the cell fate of PV^+ GABAergic interneurons in the developing forebrain (Horike et al. 2005; Wang et al. 2010). Loss of MeCP2 may de-repress the transcription of Dlx5/6 gene, leading to increased PV expression in forebrain interneurons of *Mecp2* null mice (Fig. 6b).

Several lines of evidence suggest that the striatal neurochemical environment may influence the morphology of PV^+ neurons. First, blockade of γ-aminobutyric acid (GABA) release increases the axonal arbors and bouton density of fast-spiking interneurons (Wu et al. 2012). Loss of MeCP2 down-regulates the expression of GABA synthetic enzymes and reduces GABA content in the striatum (Chao et al. 2010), which may in turn disrupts synaptic pruning and leads to overgrowth of PV^+ neuronal branches (Fig. 5c–d'). Alternatively, depletion of dopamine may remodel the formation of interneuronal microcircuits in the striatum. Using paired recordings and morphological analysis, PV^+ neurons were found to exhibit more dense and complex axonal arbors, which form new synaptic connections with DRD2-expressing MSNs after dopamine depletion (Gittis et al. 2011). In *Mecp2* null mice, dopamine is significantly reduced in the rostral striatum (Fig. 2), suggesting that reorganization of inhibitory microcircuits may enhance connections between PV^+ interneurons and DRD2-expressing MSNs of the indirect pathway. In view of the cellular function of PV which binds with calcium resulting in fast decay of intracellular Ca^{++} and delayed neurotransmitter release (Collin et al. 2005), elevated intracellular PV expression in PV^+ interneurons may chelate more calcium and diminish GABA release to DRD2-expressing MSNs, which results in dis-inhibition of the indirect pathway and impede motor activity in *Mecp2* null mice (Fig. 6b).

Notably, a larger increase in the number of PV^+ interneurons was found in the dmST than dlST in *Mecp2* null mice compared with the WT controls (Fig. 5f, g). Given that the neurons in the dmST are functionally linked to the associative corticostriatal loop involved in flexible goal-directed movement control and early phase of motor learning (Yin et al. 2009; Kimchi and Laubach 2009), the striking increase of PV^+ interneurons in the dmST may be responsible for the deficits of goal-directed behaviors and motor learning initiation in RTT. We also observed a robust increase of PV^+ neurons in the NAc of *Mecp2* null mice (Fig. 5h). In view of the fact that mice with deficient MeCP2 show reduced psychostimulant-induced behaviors and elevated threshold of sucrose preference (Deng et al. 2010), the increased number of PV^+ interneurons in the NAc may interfere the reward-related neural circuits in $Mecp2^{-/y}$ mice. The MeCP2-mediated suppression of PV^+ inhibitory interneurons in the NAc may thus play a role in modulating reward-related behaviors in vivo.

Conclusion

A striking symptom of RTT is the loss of psychomotor control. Using *Mecp2* null mice that recapitulate the psychomotor deficits of RTT, we found that a set of striatal features including the expression of striosome-specific protein MOR1, matrix neuron-enriched calcium binding protein CB, and the total number of PV^+ interneurons, are altered in the absence of MeCP2. In addition, we found that MeCP2 is required to maintain the proper level of dopamine content and the expression of genes involved in dopamine signaling such as *Th* and *Drd2*, particularly in the rostral striatum. Our study supports that MeCP2-mediated modulation of motor output through multiple pathways, either simultaneously or sequentially, in the striatum underlies the neural mechanisms by which loss of MeCP2 disrupts psychomotor function (Fig. 6). Our study provides a neural basis for the development of striatum-directed preventive and therapeutic strategies to target motor deficits in RTT, and offers insights into the structure and function of the striatum modulated by MeCP2. Further studies with a conditional genetic approach are needed to evaluate the necessary or sufficient role of striatal MeCP2 in preserving striatal structure and modulating psychomotor function.

Acknowledgments We thank Dr. Jin-Chung Chen and Dr. Ming-Ji Fann for critical reading of the manuscript, and Dr. Chih-Chang Chao for technical consultation. This study was supported by National Science Council of Taiwan (NSC99-2320-B-004-001-MY2, NSC100-2320-B-004-001, NSC101-2320-B-004-003-MY2).

Conflict of interest The authors declare that they have no conflict of interest.

References

Amir RE, Van den Veyver IB, Wan M, Tran CQ, Francke U, Zoghbi HY (1999) Rett syndrome is caused by mutations in X-linked MECP2, encoding methyl-CpG-binding protein 2. Nat Genet 23:185–188

Amir RE, Van den Veyver IB, Schultz R, Malicki DM, Tran CQ, Dahle EJ, Philippi A, Timar L, Percy AK, Motil KJ, Lichtarge O, Smith EO, Glaze DG, Zoghbi HY (2000) Influence of mutation type and X chromosome inactivation on Rett syndrome phenotypes. Ann Neurol 47:670–679

Anzalone A, Lizardi-Ortiz JE, Ramos M, De MC, Hopf FW, Iaccarino C, Halbout B, Jacobsen J, Kinoshita C, Welter M, Caron MG, Bonci A, Sulzer D, Borrelli E (2012) Dual control of

dopamine synthesis and release by presynaptic and postsynaptic dopamine D2 receptors. J Neurosci 32:9023–9034
Barmack NH, Qian Z, Yakhnittsa V (2010) Climbing fibers induce microRNA transcription in cerebellar Purkinje cells. Neuroscience 171(3):655–665
Burkett JP, Spiegel LL, Inoue K, Murphy AZ, Young LJ (2011) Activation of mu-opioid receptors in the dorsal striatum is necessary for adult social attachment in monogamous prairie voles. Neuropsychopharmacology 36:2200–2210
Canales JJ, Graybiel AM (2000) A measure of striatal function predicts motor stereotypy. Nat Neurosci 3:377–383
Chahrour M, Zoghbi HY (2007) The story of Rett syndrome: from clinic to neurobiology. Neuron 56:422–437
Chahrour M, Jung SY, Shaw C, Zhou X, Wong ST, Qin J, Zoghbi HY (2008) MeCP2, a key contributor to neurological disease, activates and represses transcription. Science 320:1224–1229
Chao HT, Chen H, Samaco RC, Xue M, Chahrour M, Yoo J, Neul JL, Gong S, Lu HC, Heintz N, Ekker M, Rubenstein JL, Noebels JL, Rosenmund C, Zoghbi HY (2010) Dysfunction in GABA signalling mediates autism-like stereotypies and Rett syndrome phenotypes. Nature 468:263–269
Chen RZ, Akbarian S, Tudor M, Jaenisch R (2001) Deficiency of methyl-CpG binding protein-2 in CNS neurons results in a Rett-like phenotype in mice. Nat Genet 27:327–331
Chiron C, Bulteau C, Loc'h C, Raynaud C, Garreau B, Syrota A, Maziere B (1993) Dopaminergic D2 receptor SPECT imaging in Rett syndrome: increase of specific binding in striatum. J Nucl Med 34:1717–1721
Collin T, Chat M, Lucas MG, Moreno H, Racay P, Schwaller B, Marty A, Llano I (2005) Developmental changes in parvalbumin regulate presynaptic Ca2+ signaling. J Neurosci 25:96–107
Crittenden JR, Graybiel AM (2011) Basal ganglia disorders associated with imbalances in the striatal striosome and matrix compartments. Front Neuroanat 5:59
Deng JV, Rodriguiz RM, Hutchinson AN, Kim IH, Wetsel WC, West AE (2010) MeCP2 in the nucleus accumbens contributes to neural and behavioral responses to psychostimulants. Nat Neurosci 13:1128–1136
Di CG, Imperato A (1988) Opposite effects of mu and kappa opiate agonists on dopamine release in the nucleus accumbens and in the dorsal caudate of freely moving rats. J Pharmacol Exp Ther 244:1067–1080
Dumas TC, Powers EC, Tarapore PE, Sapolsky RM (2004) Overexpression of calbindin D (28k) in dentate gyrus granule cells alters mossy fiber presynaptic function and impairs hippocampal-dependent memory. Hippocampus 14:701–709
Dunn HG, Stoessl AJ, Ho HH, MacLeod PM, Poskitt KJ, Doudet DJ, Schulzer M, Blackstock D, Dobko T, Koop B, de Amorim GV (2002) Rett syndrome: investigation of nine patients, including PET scan. Can J Neurol Sci 29:345–357
Enomoto H, Hendy GN, Andrews GK, Clemens TL (1992) Regulation of avian calbindin-D28K gene expression in primary chick kidney cells: importance of posttranscriptional mechanisms and calcium ion concentration. Endocrinology 130:3467–3474
Figueredo-Cardenas G, Harris CL, Anderson KD, Reiner A (1998) Relative resistance of striatal neurons containing calbindin or parvalbumin to quinolinic acid-mediated excitotoxicity compared to other striatal neuron types. Exp Neurol 149:356–372
Fujiyama F, Unzai T, Nakamura K, Nomura S, Kaneko T (2006) Difference in organization of corticostriatal and thalamostriatal synapses between patch and matrix compartments of rat neostriatum. Eur J Neurosci 24:2813–2824
Gantz SC, Ford CP, Neve KA, Williams JT (2011) Loss of Mecp2 in substantia nigra dopamine neurons compromises the nigrostriatal pathway. J Neurosci 31:12629–12637
Gemelli T, Berton O, Nelson ED, Perrotti LI, Jaenisch R, Monteggia LM (2006) Postnatal loss of methyl-CpG binding protein 2 in the forebrain is sufficient to mediate behavioral aspects of Rett syndrome in mice. Biol Psychiatry 59:468–476
Gittis AH, Hang GB, LaDow ES, Shoenfeld LR, Atallah BV, Finkbeiner S, Kreitzer AC (2011) Rapid target-specific remodeling of fast-spiking inhibitory circuits after loss of dopamine. Neuron 71:858–868
Goffin D, Allen M, Zhang L, Amorim M, Wang IT, Reyes AR, Mercado-Berton A, Ong C, Cohen S, Hu L, Blendy JA, Carlson GC, Siegel SJ, Greenberg ME, Zhou Z (2012) Rett syndrome mutation MeCP2 T158A disrupts DNA binding, protein stability and ERP responses. Nat Neurosci 15:274–283
Graybiel AM (1984) Correspondence between the dopamine islands and striosomes of the mammalian striatum. Neuroscience 13:1157–1187
Guy J, Hendrich B, Holmes M, Martin JE, Bird A (2001) A mouse Mecp2-null mutation causes neurological symptoms that mimic Rett syndrome. Nat Genet 27:322–326
Hagberg B, Aicardi J, Dias K, Ramos O (1983) A progressive syndrome of autism, dementia, ataxia, and loss of purposeful hand use in girls: Rett's syndrome: report of 35 cases. Ann Neurol 14:471–479
Herkenham M, Pert CB (1981) Mosaic distribution of opiate receptors, parafascicular projections and acetylcholinesterase in rat striatum. Nature 291:415–418
Hilario M, Holloway T, Jin X, Costa RM (2012) Different dorsal striatum circuits mediate action discrimination and action generalization. Eur J Neurosci 35:1105–1114
Hontanilla B, de las HS, Gimenez-Amaya JM (1996) A topographic re-evaluation of the nigrostriatal projections to the caudate nucleus in the cat with multiple retrograde tracers. Neuroscience 72:485–503
Horike S, Cai S, Miyano M, Cheng JF, Kohwi-Shigematsu T (2005) Loss of silent-chromatin looping and impaired imprinting of DLX5 in Rett syndrome. Nat Genet 37:31–40
Hwang CK, Song KY, Kim CS, Choi HS, Guo XH, Law PY, Wei LN, Loh HH (2009) Epigenetic programming of mu-opioid receptor gene in mouse brain is regulated by MeCP2 and Brg1 chromatin remodelling factor. J Cell Mol Med 13:3591–3615
Johnson SW, North RA (1992) Opioids excite dopamine neurons by hyperpolarization of local interneurons. J Neurosci 12:483–488
Jouvenceau A, Potier B, Poindessous-Jazat F, Dutar P, Slama A, Epelbaum J, Billard JM (2002) Decrease in calbindin content significantly alters LTP but not NMDA receptor and calcium channel properties. Neuropharmacology 42:444–458
Jung MY, Hof PR, Schmauss C (2000) Targeted disruption of the dopamine D(2) and D(3) receptor genes leads to different alterations in the expression of striatal calbindin-D(28k). Neuroscience 97:495–504
Kimchi EY, Laubach M (2009) Dynamic encoding of action selection by the medial striatum. J Neurosci 29:3148–3159
Koos T, Tepper JM (1999) Inhibitory control of neostriatal projection neurons by GABAergic interneurons. Nat Neurosci 2:467–472
Kreitzer AC, Malenka RC (2008) Striatal plasticity and basal ganglia circuit function. Neuron 60:543–554
Lang M, Wither RG, Brotchie JM, Wu C, Zhang L, Eubanks JH (2013) Selective preservation of MeCP2 in catecholaminergic cells is sufficient to improve the behavioral phenotype of male and female Mecp2-deficient mice. Hum Mol Genet 22:358–371
Lawhorn C, Smith DM, Brown LL (2009) Partial ablation of mu-opioid receptor rich striosomes produces deficits on a motor-skill learning task. Neuroscience 163:109–119
Liao WL, Tsai HC, Wang HF, Chang J, Lu KM, Wu HL, Lee YC, Tsai TF, Takahashi H, Wagner M, Ghyselinck NB, Chambon P, Liu FC (2008) Modular patterning of structure and function of

the striatum by retinoid receptor signaling. Proc Natl Acad Sci USA 105:6765–6770

Lindgren N, Xu ZQ, Herrera-Marschitz M, Haycock J, Hokfelt T, Fisone G (2001) Dopamine D(2) receptors regulate tyrosine hydroxylase activity and phosphorylation at Ser40 in rat striatum. Eur J Neurosci 13:773–780

Liu FC, Graybiel AM (1992) Transient calbindin-D28k-positive systems in the telencephalon: ganglionic eminence, developing striatum and cerebral cortex. J Neurosci 12:674–690

Miralves J, Magdeleine E, Joly E (2007) Design of an improved set of oligonucleotide primers for genotyping MeCP2tm1.1Bird KO mice by PCR. Mol Neurodegener 2:16

Miura M, Saino-Saito S, Masuda M, Kobayashi K, Aosaki T (2007) Compartment-specific modulation of GABAergic synaptic transmission by mu-opioid receptor in the mouse striatum with green fluorescent protein-expressing dopamine islands. J Neurosci 27:9721–9728

Moles A, Kieffer BL, D'Amato FR (2004) Deficit in attachment behavior in mice lacking the mu-opioid receptor gene. Science 304:1983–1986

Moore AE, Cicchetti F, Hennen J, Isacson O (2001) Parkinsonian motor deficits are reflected by proportional A9/A10 dopamine neuron degeneration in the rat. Exp Neurol 172:363–376

Mosconi MW, Takarae Y, Sweeney JA (2011) Motor functioning and dyspraxia in autism spectrum disorders. In: Amaral DG, Dawson G, Geschwind DH (eds) Autism spectrum disorders. Oxford University Press Inc, New York, pp 355–380

Nan X, Ng HH, Johnson CA, Laherty CD, Turner BM, Eisenman RN, Bird A (1998) Transcriptional repression by the methyl-CpG-binding protein MeCP2 involves a histone deacetylase complex. Nature 393:386–389

Pan PY, Ryan TA (2012) Calbindin controls release probability in ventral tegmental area dopamine neurons. Nat Neurosci 15:813–815

Panayotis N, Pratte M, Borges-Correia A, Ghata A, Villard L, Roux JC (2011) Morphological and functional alterations in the substantia nigra pars compacta of the Mecp2-null mouse. Neurobiol Dis 41:385–397

Paxinos and Franklin (2004) The mouse brain in stereotaxic coordinates. Compact second edition. Elsevier, London

Piepponen TP, Honkanen A, Kivastik T, Zharkovsky A, Turtia A, Mikkola JA, Ahtee L (1999) Involvement of opioid mu1-receptors in opioid-induced acceleration of striatal and limbic dopaminergic transmission. Pharmacol Biochem Behav 63:245–252

Reiss AL, Faruque F, Naidu S, Abrams M, Beaty T, Bryan RN, Moser H (1993) Neuroanatomy of Rett syndrome: a volumetric imaging study. Ann Neurol 34:227–234

Samaco RC, Mandel-Brehm C, Chao HT, Ward CS, Fyffe-Maricich SL, Ren J, Hyland K, Thaller C, Maricich SM, Humphreys P, Greer JJ, Percy A, Glaze DG, Zoghbi HY, Neul JL (2009) Loss of MeCP2 in aminergic neurons causes cell-autonomous defects in neurotransmitter synthesis and specific behavioral abnormalities. Proc Natl Acad Sci USA 106:21966–21971

Samaco RC, Mandel-Brehm C, McGraw CM, Shaw CA, McGill BE, Zoghbi HY (2012) Crh and Oprm1 mediate anxiety-related behavior and social approach in a mouse model of MECP2 duplication syndrome. Nat Genet 44:206–211

Schmidt H (2012) Three functional facets of calbindin D-28k. Front Mol Neurosci 5:25

Shahbazian MD, Antalffy B, Armstrong DL, Zoghbi HY (2002a) Insight into Rett syndrome: MeCP2 levels display tissue-and cell-specific differences and correlate with neuronal maturation. Hum Mol Genet 11:115–124

Shahbazian M, Young J, Yuva-Paylor L, Spencer C, Antalffy B, Noebels J, Armstrong D, Paylor R, Zoghbi H (2002b) Mice with truncated MeCP2 recapitulate many Rett syndrome features and display hyperacetylation of histone H3. Neuron 35:243–254

Stearns NA, Schaevitz LR, Bowling H, Nag N, Berger UV, Berger-Sweeney J (2007) Behavioral and anatomical abnormalities in Mecp2 mutant mice: a model for Rett syndrome. Neuroscience 146:907–921

Sterling L, McLaughlin A, King BH (2011) Stereotypy and self-injury. In: Amaral DG, Dawson G, Geschwind DH (eds) Autism spectrum disorder. Oxford University Press Inc, New York, pp 339–354

Szulwach KE, Li X, Smrt RD, Li Y, Luo Y, Lin L, Santistevan NJ, Li W, Zhao X, Jin P (2010) Cross talk between microRNA and epigenetic regulation in adult neurogenesis. J Cell Biol 189(1):127–141

Temudo T, Ramos E, Dias K, Barbot C, Vieira JP, Moreira A, Calado E, Carrilho I, Oliveira G, Levy A, Fonseca M, Cabral A, Cabral P, Monteiro JP, Borges L, Gomes R, Santos M, Sequeiros J, Maciel P (2008) Movement disorders in Rett syndrome: an analysis of 60 patients with detected MECP2 mutation and correlation with mutation type. Mov Disord 23:1384–1390

Thorn CA, Atallah H, Howe M, Graybiel AM (2010) Differential dynamics of activity changes in dorsolateral and dorsomedial striatal loops during learning. Neuron 66:781–795

Ungerstedt U, Herrera-Marschitz M, Stahle L, Tossman U, Zetterstrom T (1985) Functional classification of different dopamine receptors. Psychopharmacology Suppl 2:19–30

van der Kooy D, Fishell G (1992) Embryonic lesions of the substantia nigra prevent the patchy expression of opiate receptors, but not the segregation of patch and matrix compartment neurons, in the developing rat striatum. Brain Res Dev Brain Res 66:141–145

Wang Y, Dye CA, Sohal V, Long JE, Estrada RC, Roztocil T, Lufkin T, Deisseroth K, Baraban SC, Rubenstein JL (2010) Dlx5 and Dlx6 regulate the development of parvalbumin-expressing cortical interneurons. J Neurosci 30:5334–5345

Watabe-Uchida M, Zhu L, Ogawa SK, Vamanrao A, Uchida N (2012) Whole-brain mapping of direct inputs to midbrain dopamine neurons. Neuron 74:858–873

Wood L, Shepherd GM (2010) Synaptic circuit abnormalities of motor-frontal layer 2/3 pyramidal neurons in a mutant mouse model of Rett syndrome. Neurobiol Dis 38:281–287

Wood L, Gray NW, Zhou Z, Greenberg ME, Shepherd GM (2009) Synaptic circuit abnormalities of motor-frontal layer 2/3 pyramidal neurons in an RNA interference model of methyl-CpG-binding protein 2 deficiency. J Neurosci 29:12440–12448

Wu Y, Parent A (2000) Striatal interneurons expressing calretinin, parvalbumin or NADPH-diaphorase: a comparative study in the rat, monkey and human. Brain Res 863:182–191

Wu X, Fu Y, Knott G, Lu J, Di CG, Huang ZJ (2012) GABA signaling promotes synapse elimination and axon pruning in developing cortical inhibitory interneurons. J Neurosci 32:331–343

Yenari MA, Minami M, Sun GH, Meier TJ, Kunis DM, McLaughlin JR, Ho DY, Sapolsky RM, Steinberg GK (2001) Calbindin d28k overexpression protects striatal neurons from transient focal cerebral ischemia. Stroke 32:1028–1035

Yin HH, Mulcare SP, Hilario MR, Clouse E, Holloway T, Davis MI, Hansson AC, Lovinger DM, Costa RM (2009) Dynamic reorganization of striatal circuits during the acquisition and consolidation of a skill. Nat Neurosci 12:333–341